RESEARCH ARTICLE

Design and Optimization of Colon-Targeted Multiparticulate Nanosponges of Metronidazole for Enhanced Release and Stability

Shubhangi B Khade*, Raosaheb S Shendge

Department of Pharmaceutics, Sanjivani College of Pharmaceutical Education and Research, Savitribai Phule Pune University, Sahajanand Nagar, Shingnapur, Kopargaon, Ahmednagar, Maharashtra-423603, India

Received: 16th Jun, 2025; Revised: 20th Jul, 2025; Accepted: 29th Jul, 2025; Available Online: 25th Sep, 2025

ABSTRACT

This work sought to formulate and optimize Metronidazole-loaded nanosponges to improve solubility, entrapment efficiency, and sustained release. Nanosponges were synthesized by the emulsion solvent evaporation technique and optimized utilizing a central composite design. Among 20 formulations, batch F9 demonstrated excellent results with a mean particle size of 200.78 nm, a zeta potential of −31.7 mV, and a polydispersity index of 0.205, signifying a uniform nanosized dispersion. The entrapment efficiency varied between 81.55% and 85.95%, with formulation F9 exhibiting the greatest efficiency at 85.95 ± 0.95% and a drug loading capacity of 79.53 ± 0.13%. *In-vitro* release tests indicated sustained drug release, with F9 attaining 95.15 ± 1.20% release within 12 hours, adhering to zero-order kinetics (R^2 = 0.9973) and a Higuchi diffusion-controlled mechanism (R^2 = 0.9217). Capsule formulation of the optimized batch showed consistent drug content (99.15 ± 0.02%) and stability over 90 days without significant changes in release profile (94.10 ± 0.01% at 3 months). These findings suggest that nanosponge-based delivery of Metronidazole offers improved solubility, entrapment, and sustained release with good stability, making it a promising approach for effective oral drug delivery.

Keywords: Metronidazole; Nanosponges; Central Composite Design; Entrapment Efficiency; Sustained Release; Drug Stability

How to cite this article: Shubhangi B Khade, Raosaheb S Shendge. Design and Optimization of Colon-Targeted Multiparticulate Nanosponges of Metronidazole for Enhanced Release and Stability. International Journal of Drug Delivery Technology. 2025;15(3):1187-97. doi: 10.25258/ijddt.15.3.38

Source of support: Nil.

Conflict of interest: None

INTRODUCTION

Oral drug delivery remains the most widely accepted and convenient route of administering therapeutic agents due to its simplicity, high patient compliance, non-invasiveness, and cost-effectiveness[1,2]. However, despite these advantages, a large proportion of APIs face significant challenges when administered orally, including poor aqueous solubility, erratic bioavailability, rapid metabolism, and premature degradation in the gastrointestinal tract. Such limitations often result in suboptimal absorption, variable plasma drug concentrations, and reduced therapeutic outcomes. Drugs with low solubility typically exhibit limited dissolution in gastrointestinal fluids, which directly affects the rate and extent of absorption, ultimately diminishing their clinical efficacy[3-5]. Therefore, addressing these pharmacokinetic and biopharmaceutical challenges requires the development of advanced drug delivery strategies that can enhance solubility, improve stability, and provide controlled or targeted release.

Metronidazole, a widely prescribed nitroimidazole derivative, is an effective antibacterial and antiprotozoal agent. It is routinely used in the management of infections such as bacterial vaginosis, trichomoniasis, amebiasis, giardiasis, and Helicobacter pylori–induced gastrointestinal infections[6,7]. Despite its extensive clinical utility, Metronidazole exhibits limitations that compromise its therapeutic potential, including poor aqueous solubility, a relatively short half-life, and gastrointestinal side effects associated with conventional oral formulations. Regular dosage is often necessary to sustain therapeutic plasma concentrations, potentially leading to patient non-compliance and variable drug levels, which diminishes effectiveness and heightens the risk of side effects[8-11]. These limitations underscore the pressing need for novel formulation strategies that might improve solubility, extend systemic exposure, and reduce dosing frequency.

In recent years, nanotechnology-based medication delivery technologies have arisen as potential solutions to address these restrictions. Nanosponges have garnered significant interest owing to their distinctive structural and functional characteristics[12-14].

Nanosponges are extensively cross-linked, three-dimensional porous polymeric structures that may encapsulate a diverse array of medicinal compounds, including both hydrophilic and hydrophobic substances. Their nanoscale size and large surface area facilitate improved solubility and stability of poorly water-soluble pharmaceuticals. The porous structure of nanosponges facilitates regulated and sustained release, minimizing dose frequency and preserving therapeutic drug levels for prolonged durations. In addition to these advantages, nanosponge formulations provide substantial drug-loading capacity, biocompatibility, low toxicity, and safeguard

**Author for Correspondence: Shubhangi.gite21@gmail.com*

labile pharmaceuticals against chemical or enzymatic breakdown inside the gastrointestinal atmosphere[15-18].

Many research investigations have shown the effectiveness of nanosponge-based devices in enhancing the bioavailability of poorly soluble pharmaceuticals, extending drug release profiles, and minimizing undesirable side effects. Specifically, for antimicrobial agents like Metronidazole, nanosponge formulations can substantially enhance solubility, facilitate targeted or site-specific delivery, and provide sustained release, thereby improving therapeutic outcomes and patient adherence. Optimizing formulation parameters such as polymer concentration, cross-linking density, stabilizer type and concentration, and processing conditions can further influence particle size, entrapment efficiency, and drug release kinetics, enabling precise tailoring of the system to meet specific therapeutic needs.

The present study aims to design and optimize colon-targeted multiparticulate nanosponges of Metronidazole, focusing on improving drug solubility, stability, and therapeutic efficacy. By leveraging the advantages of nanosponge carriers and optimizing formulation variables, this approach seeks to achieve sustained drug release, minimize gastrointestinal side effects, and reduce dosing frequency. Ultimately, this formulation strategy offers a promising alternative to conventional Metronidazole delivery systems, providing enhanced patient compliance, improved pharmacokinetic profiles, and a potentially superior therapeutic outcome in the treatment of gastrointestinal and systemic infections.

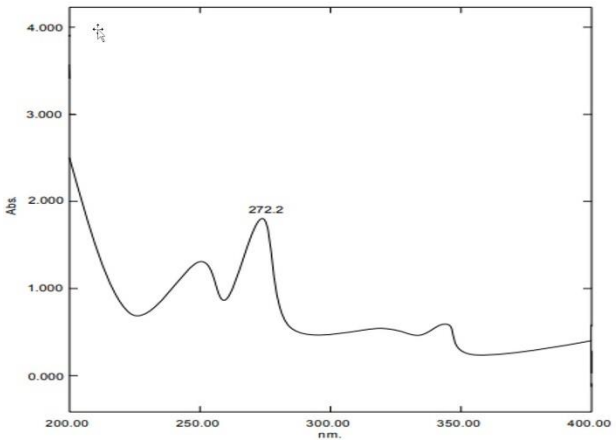

Figure 1. UV spectrum of Metronidazole

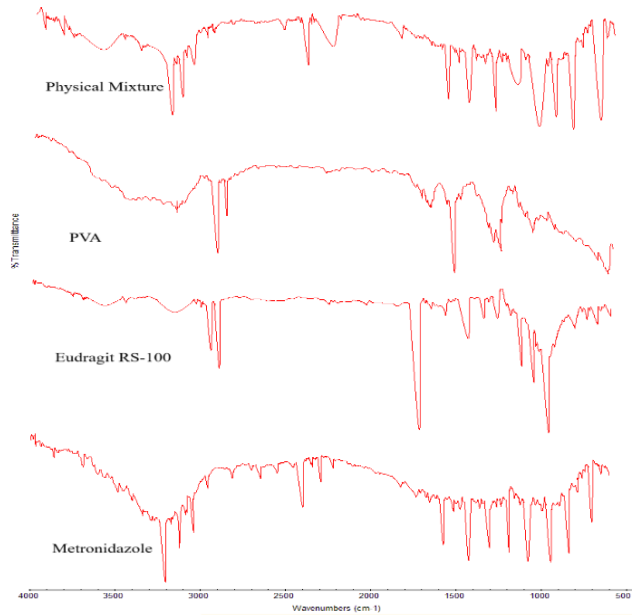

Figure 2: FTIR spectra of Metronidazole, Eudragit RS-100, PVA, and Physical Mixture

MATERIAL AND METHOD

Materials

Metronidazole was kindly provided as a gift sample by Hetero Drugs, Hyderabad, India. Eudragit RS-100 was generously supplied by Lee Pharma Limited, Visakhapatnam, India. All other solvents, polyvinyl alcohol, and auxiliary chemicals of analytical reagent grade were obtained from SDFCL, Mumbai, and were used as received without any further purification.

Methods

Identification and Confirmation of Drug

The identity and purity of the drug were confirmed through melting point determination, FTIR spectroscopy (Shimadzu 8400S, Japan), and DSC (METTLER STAR SW 12.10). The melting point analysis provided the preliminary confirmation of the drug by comparing its characteristic melting behaviour, while FTIR spectroscopy was used to identify functional groups and verify the structural integrity of the compound. In addition, DSC was used to study the thermal behaviour and confirm the crystalline nature and purity of the drug. Together, these techniques ensured accurate identification and reliable confirmation of the drug[19-21].

Solubility, Drug-polymer Compatibility, and Nanosponges Optimization

Solubility is a crucial parameter influencing bioavailability, as drugs with solubility below 10 mg/mL may face absorption issues.

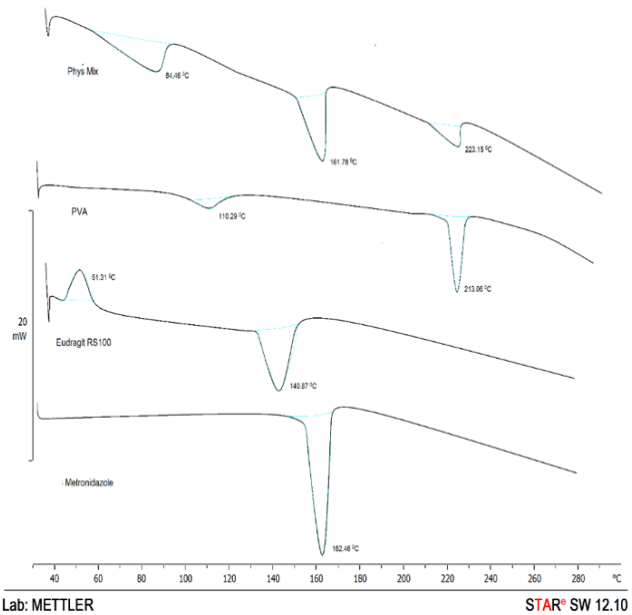

Figure 3: DSC thermograms of Metronidazole, Eudragit RS-100, PVA, and Physical Mixture

Table 1. Design Variables

Variables	Levels		
Independent	Eudragit RS-100 (X_1) Levels: Low: 100mg and High: 200mg	PVA (X_2) Levels: Low: 50mg and High: 100mg	Swirling speed (X_3) Levels: Low: 500RPM and High: 1000RPM
Dependent	Particle Size (nm) (Y_1)	Entrapment Efficiency (%EE) (Y_2)	%Drug Release (Y_3)

Table 2. Formulations Batches as per RSM-CCD design

Formu-lation Code	Metronidazole (mg)	Eudragit RS-100 (mg)	PVA (mg)	Swirling speed (RPM)
F-1	15mg	150	75	750
F-2		150	75	750
F-3		150	32.9552	750
F-4		100	100	500
F-5		150	75	750
F-6		65.9104	75	750
F-7		200	50	1000
F-8		150	75	750
F-9		100	50	500
F-10		150	75	1170.45
F-11		200	50	500
F-12		100	50	1000
F-13		150	75	750
F-14		100	100	1000
F-15		277.09	75	750
F-16		150	75	750
F-17		200	100	500
F-18		200	100	1000
F-19		150	75	329.552
F-20		150	117.045	750

Table 3. Solubility data of Metronidazole

Medium		Solubility (mg/ml)
Distilled Water		0.935 ± 0.08
Methanol		8.251 ± 0.05
Phosphate buffer	pH-1.2	0.325 ± 0.09
	pH-6.8	9.981 ± 0.07

Table 4. Design Batches

Formu-lation Code	X_1 (mg)	X_2 (mg)	X_3 (RPM)	Y_1 (nm)	Y_2 (%)	Y_3 (%)
F1	150	75	750	350.24	81.95	91.85
F2	150	75	750	345.12	81.72	91.74
F3	150	32.9552	750	280.45	83.25	93.5
F4	100	100	500	315.78	83.55	93.65
F5	150	75	750	348.21	81.61	91.92
F6	65.9104	75	750	278.95	83.95	93.45
F7	200	50	1000	370.45	82.85	92.9
F8	150	75	750	350.85	82.68	92.58
F9	100	50	500	200.78	85.95	95.15
F10	150	75	1170.45	375.65	84.05	92.9
F11	200	50	500	275.34	83.25	93.12
F12	100	50	1000	290.12	83.48	93.28
F13	150	75	750	350.65	81.82	91.85
F14	100	100	1000	360.45	83.15	92.05
F15	277.09	75	750	275.78	83.92	93.65
F16	150	75	750	355.45	81.55	91.72
F17	200	100	500	385.35	82.45	92.6
F18	200	100	1000	375.12	84.15	93.82
F19	150	75	329.552	275.42	83.82	93.52
F20	150	117.045	750	375.15	83.28	93.9

The solubility of Metronidazole was evaluated in ethanol, water, and pH 6.8 buffer at 37±0.5°C by adding an excess of the drug to 10 mL of solvent in glass vials with rubber closures, followed by shaking in an orbital incubator (Remi CIS-18; Remi Pvt. Ltd., India) for 24 hours and equilibrium maintenance at 37±0.5°C for 12 hours. The solutions were filtered through a 0.45 µm Millipore filter, and the filtrate was analyzed using UV spectroscopy at λmax 272 nm with a calibration curve to determine solubility. Drug-polymer compatibility was assessed using FTIR and DSC. FTIR analyzed the absorption spectra of the pure drug, excipients, and physical mixtures to detect potential chemical interactions or functional group alterations, while DSC examined thermal properties, including melting point, crystallinity, and stability, to evaluate any changes upon mixing with excipients[22]. Nanosponges optimization was performed using RSM-CCD with three independent variables—Eudragit RS-100 quantity (X1), PVA quantity (X2), and swirling speed (X3)—while keeping other formulation parameters constant. Design Expert 13 (Stat-Ease 13.0.3.1) software was used to develop 20 formulations (F1–F20) and generate a polynomial equation. The response variables examined were particle size (Y1), entrapment efficiency (%EE, Y2), and % drug release (Y3), as summarized in Table 1.

Model-validation and Optimization of Data

ANOVA was performed to evaluate the statistical significance and reliability of the polynomial equations generated using Design Expert® Software[23,24]. A multiple linear regression model applied to the RSM-based design produced a predictive equation incorporating both interaction and higher-order polynomial terms, essential for accurately interpreting the experimental responses. Here, Y represents the observed response for each combination of factor levels, b0 is the intercept reflecting the overall mean of all nine trials, and the coefficients bi (b1, b2, b11, b12, b22) are regression parameters estimated from the data. X1, X2, and X3 denote the coded independent variables in the design matrix.

Preparation of METRO Nanosponges

METRO nanosponges (F1-F20) were produced using the emulsion solvent evaporation technique, as outlined in Table 2. Eudragit-RS100 functioned as the polymer, whereas PVA acted as the surfactant in the assessment of polymer and surfactant concentrations. The organic phase was produced by dissolving designated amounts of Eudragit-RS100 and METRO in dichloromethane. PVA was soluble in 100 milliliters of purified water to create aqueous phase. Two phases were combined by gradually adding an organic phase to constant aqueous phase during stirring for two hours at 1000 rpm. The generated

nanosponges underwent vacuum filtration and were subsequently dried at 40ºC for 24 hr prior to storing in a desiccator.

Evaluation of Optimized Nanosponges Formulation

Particle Size, ZP, and PDI

Characterization of Nanosponges: Particle Size, Zeta Potential, PDI, and Drug Loading

The particle size distribution, PDI, and ZP of the nanosponge formulations were measured using a Zetasizer (Malvern Nano ZS) at 25 ± 0.5 °C, with samples appropriately diluted in distilled water for accurate analysis. The %EE and drug loading (%DL) were determined by dispersing 50 mg of nanosponges in 10 mL phosphate buffer (pH 6.8) with continuous agitation until complete dissolution. The clear supernatant was collected, and the concentration of METRO was quantified using a UV–visible spectrophotometer.

XRD, DSC and SEM Analysis

The formulated nanosponges underwent a series of characterization studies to comprehensively assess their physicochemical, thermal, and morphological attributes. XRD analysis was carried out to investigate whether Metronidazole existed in a crystalline or amorphous state within the nanosponge matrix[25,26]. DSC was utilized to evaluate the thermal characteristics and identify possible phase transitions of the prepared samples[27]. Furthermore, SEM a comprehensive analysis of the surface characteristics and structural architecture of the developed formulation[28,29].

In-vitro Drug Release Study

The drug release profile was evaluated with a USP-II dissolving device (paddle technique, Labtronics). The experiment was conducted under regulated circumstances at a temperature of 37 ± 0.2 °C. A 900 mL volume of phosphate buffer (pH 6.8) was used as the dissolving media, sustained at a paddle rotation speed of 100 rpm. Fifteen milligrams of nanosponges containing the medicine were precisely measured, encapsulated in a diffusion sachet, and then placed into the dissolving tank. Samples were extracted at specified time intervals ranging from 1 to 12 hours, thereafter analyzed for drug concentration by UV-VIS spectrophotometry at 272 nm.

Preformulation Studies of Nanosponges

The flow properties, including angle of repose, bulk density, tapped density, compressibility index, and Hausner's ratio, of the optimized formulation were systematically assessed to evaluate its appropriateness and suitability for capsule development[30,31].

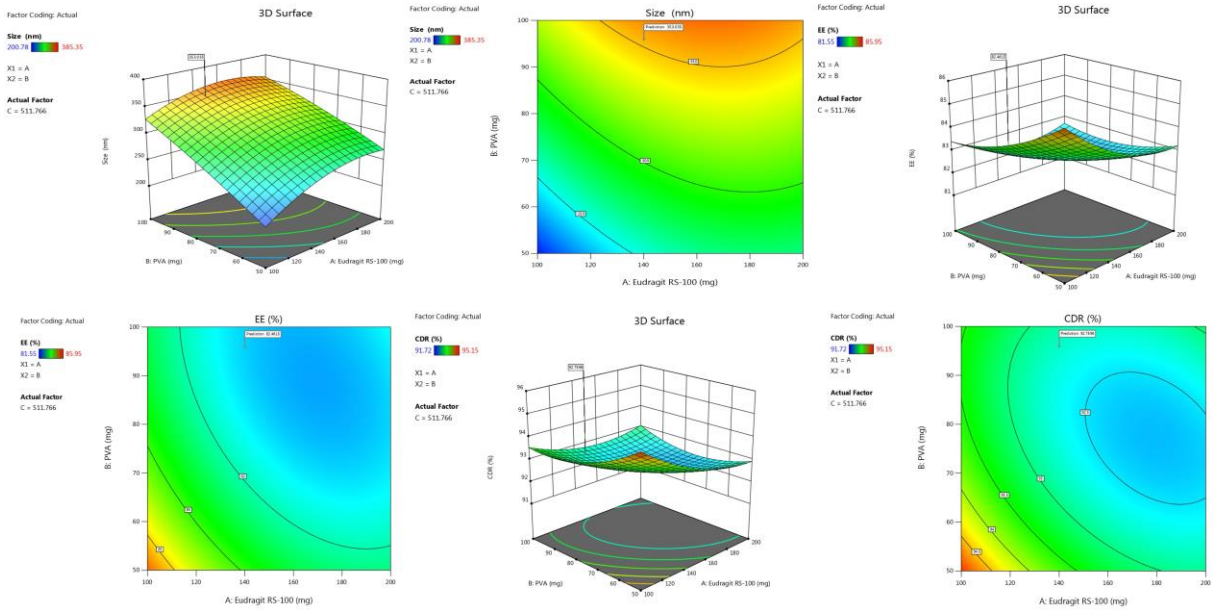

Figure 4: Three-dimensional RSPs

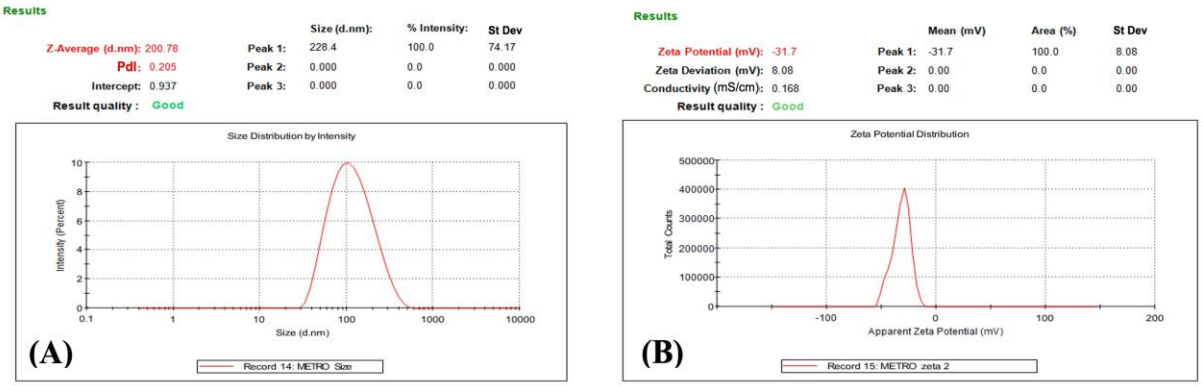

Figure 5: (A) Particle size; (B) ZP of F9 batch

Formulation of Capsule using Optimized Nanosponges

Metronidazole-loaded nanosponges were successfully prepared through the emulsion solvent evaporation technique, employing Eudragit RS-100 as the polymer matrix and PVA as a stabilizer as well as surfactant, and the final formulation was encapsulated within hard gelatin capsules.

Evaluation of Metronidazole Nanosponges Capsules

Uniformity of Weight and Drug Content Determination

The uniformity of weight of capsules was assessed by initially weighing intact capsules with precision. Size Zero capsules were carefully opened to remove their contents, and the shells were rinsed with ether to eliminate residual material, then left to dry until the solvent odor dissipated before reweighing[32]. The mean weight was calculated,

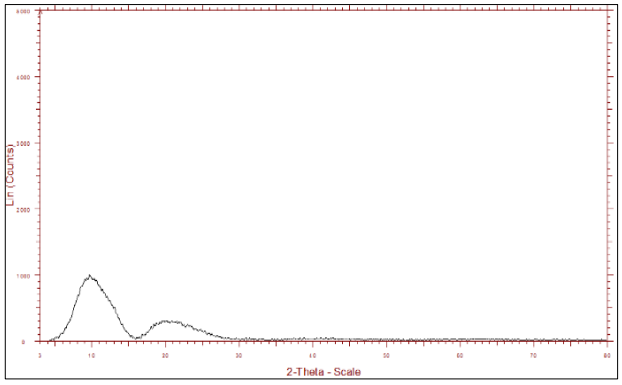

Figure 6: XRD of F9 batch

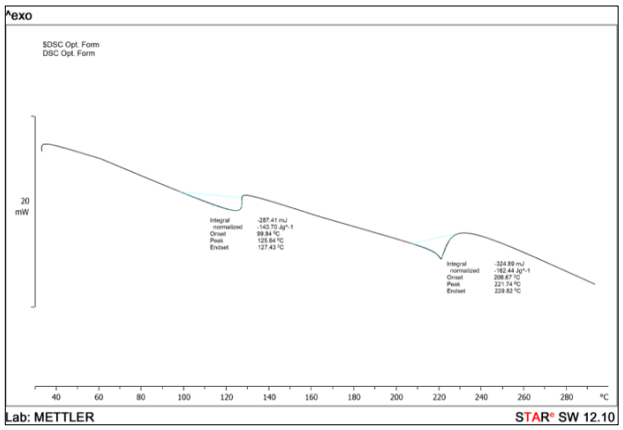

Figure 7: DSC of F9 batch

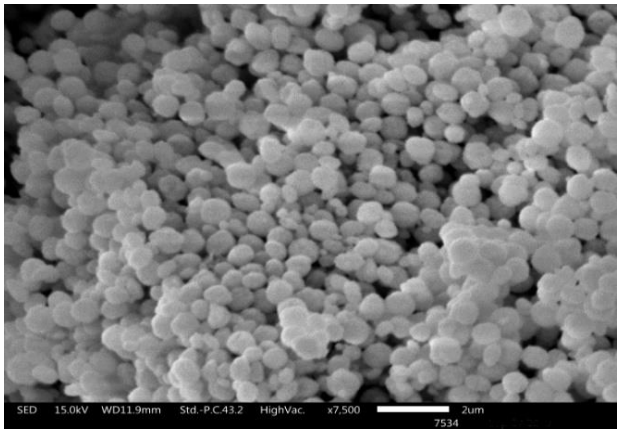

Figure 8: SEM image of F9 batch

ensuring that no more than two individual capsule weights deviated from the mean beyond the permitted variation, and none exceeded twice that limit. For drug content analysis, five capsules were randomly selected, and their average weight determined. An accurately measured 15 mg portion of the powdered Metronidazole was diluted to 100 mL with phosphate buffer (pH 6.8) and left overnight for complete solubilization. From this solution, 1 mL was further diluted to 50 mL with the same buffer, and the absorbance was measured at 272 nm using a suitable spectrophotometric method.

In-vitro Drug Release Study

The *in-vitro* drug release investigation of Metronidazole-loaded nanosponges capsules was carried out following the previously outlined procedure specific to nanosponge formulations, ensuring consistency and reliability of the experimental approach.

Kinetics of Drug Release

The drug release kinetics from the formulated preparations were thoroughly assessed using several mathematical models to clarify the processes driving release. Zero-order and first-order models were used to ascertain if the drug was released at a consistent rate throughout time or whether the release was contingent upon the residual drug concentration in the system. The Higuchi model was used to examine diffusion-controlled drug release via the matrix, while the Korsmeyer–Peppas model offered more insights into the release process by evaluating the release exponent (n value). The experimental release data were fitted to these models, allowing for a full characterization of the overall release profile and the primary mechanism governing drug release.

Stability Studies

The stability of Metronidazole nanosponges capsules was rigorously assessed over 90 days under ambient environments and regulated relative humidity (40°C/75% RH). At specified intervals, samples were extracted and underwent thorough characterization, including evaluation of physical appearance, drug content, and *in-vitro* dissolution.

RESULTS AND DISCUSSION

Drug Identification and Verification

Determination of Melting Point

The melting point of Metronidazole was determined using three different methods: the glass capillary method, a melting point apparatus, and DSC. Using the glass capillary method, the observed melting point ranged from 145 to 148°C. The melting point apparatus showed a slightly narrower range of 146 to 148°C. DSC analysis revealed a precise melting temperature of 147.54°C. The experimentally determined values were in agreement with the conventional melting point of Metronidazole.

UV Analysis

The Metronidazole solution was examined by scanning from 400-200 nm, demonstrating a significant absorption peak at 272 nm, as seen in Figure 1. This observation aligns with earlier documented UV-Visible spectra of Metronidazole, which also exhibited a maximum absorption at 272 nm (λ max).

Table 5. Overview of the regression study findings for response Y1, Y2, and Y3

Response Quadratic Effect	R^2	Adjusted R^2	Predicted R^2	SD	%CV
(Y_1)	0.9013	0.8125	0.2429	21.43	6.56
(Y_2)	0.9072	0.8236	0.5282	0.4581	0.5511
(Y_3)	0.8907	0.7923	0.3513	0.0016	0.4502

FTIR Studies

The chemical's spectra exhibit significant absorption bands confirm the presence of its functional groups (Figure 2). The nitro (-NO_2) group exhibits characteristic strong absorption peaks, with asymmetric stretching observed around 1470 cm^{-1} and symmetric stretching near 1360 cm^{-1}. The imidazole ring is identified by a distinct C=N stretching vibration at approximately 1530 cm^{-1}, while the hydroxyl (-OH) group contributes a broad absorption band around 3200 cm^{-1}, indicative of hydrogen bonding. Any significant shifts in these peak positions may suggest molecular interactions or structural modifications in metronidazole, providing insights into its chemical environment and potential formulation changes.

DSC

The DSC thermogram of Metronidazole, obtained under a heating rate of 100 ºC/min along with continuous nitrogen purging, exhibited a distinct and sharp endothermic peak at 147.54 ºC (Figure 3). This thermal event is consistent with the reported melting point range of 146–148 ºC, thereby confirming the purity and crystalline nature of the drug.

Evaluation of Drug Solubility in Various Solvents

Table 3 illustrates the solubility of Metronidazole as a function of pH. The solubility profile suggests that the compound is poorly soluble in water but exhibits significantly increased solubility in methanol and phosphate buffer at pH 6.8.

This information is crucial for formulating the compound for biological studies or pharmaceutical applications, as choosing an appropriate solvent can enhance bioavailability and efficacy. The high solubility in phosphate buffer also suggests that the compound could have favorable solubility in biological fluids, which is advantageous for *in-vitro* studies.

Assessment of Drug-polymer Compatibility

FTIR Spectroscopy

This approach was used to determine any potential reactions between Metronidazole and Eudragit RS-100 PVA, along with their physical combinations. The spectra of Metronidazole, Eudragit RS-100, PVA, and their physical combinations are presented in Figures 1 and 8-10. The drug's spectra exhibit significant absorption peaks confirm the presence of its functional groups. The nitro (-NO_2) group exhibits characteristic strong absorption peaks, with asymmetric stretching observed around 1470 cm^{-1} and symmetric stretching near 1360 cm^{-1}. The imidazole ring is identified by a distinct C=N stretching vibration at approximately 1530 cm^{-1}, while the hydroxyl (-OH) group contributes a broad absorption band around 3200 cm^{-1}, indicative of hydrogen bonding. The FTIR spectra of the physical mixture exhibited findings similar to those of the original substance, demonstrating the absence of interaction and verifying compatibility (Figure 2).

Table 6: % EE and %DL of batches

Batch Code	%EE	DL (%)	Batch Code	%EE	DL (%)
F1	81.95 ± 1.25	70.25 ± 0.10	F11	83.25 ± 1.18	78.89 ± 0.17
F2	81.72 ± 1.30	72.92 ± 0.12	F12	83.48 ± 1.25	71.93 ± 0.19
F3	83.25 ± 1.10	73.41 ± 0.14	F13	81.82 ± 1.32	71.11 ± 0.21
F4	83.55 ± 1.15	71.25 ± 0.16	F14	83.15 ± 1.20	70.20 ± 0.22
F5	81.61 ± 1.35	71.42 ± 0.18	F15	83.92 ± 1.05	71.50 ± 0.23
F6	83.95 ± 1.05	72.32 ± 0.20	F16	81.55 ± 1.38	72.10 ± 0.24
F7	82.85 ± 1.20	75.32 ± 0.09	F17	82.45 ± 1.25	71.80 ± 0.20
F8	82.68 ± 1.28	73.11 ± 0.11	F18	84.15 ± 1.10	74.50 ± 0.25
F9	85.95 ± 0.95	79.53 ± 0.13	F19	83.82 ± 1.08	71.00 ± 0.21
F10	84.05 ± 1.10	75.21 ± 0.15	F20	83.28 ± 1.18	72.30 ± 0.22

Table 7: Drug release profile of F1-F20 nanosponges

Batch Code	CDR (%)	Batch Code	CDR (%)
F1	91.85 ± 1.08	F11	93.12 ± 1.11
F2	91.74 ± 1.09	F12	93.28 ± 1.13
F3	93.5 ± 1.11	F13	91.85 ± 1.14
F4	93.65 ± 1.13	F14	92.05 ± 1.16
F5	91.92 ± 1.15	F15	93.65 ± 1.18
F6	93.45 ± 1.17	F16	91.72 ± 1.19
F7	92.9 ± 1.19	F17	92.6 ± 1.21
F8	92.58 ± 1.10	F18	93.82 ± 1.25
F9	95.15 ± 1.20	F19	93.52 ± 1.23
F10	92.9 ± 1.22	F20	93.9 ± 1.12

DSC

The thermal behavior of the drug and excipients was evaluated using DSC. Thermograms were recorded for pure Metronidazole, Eudragit RS-100, PVA, and their physical mixture. Samples were placed in perforated aluminum pans and subjected to a controlled heating rate of 10°C/min over a temperature range of 30–300°C, as illustrated in Figure 3. DSC analysis of Metronidazole demonstrated a distinct endothermic peak at 147.54°C, which corresponds well with its reported melting range of 146–148°C, confirming its thermal stability. Eudragit RS-100 exhibited a prominent endothermic peak at 129.98°C, while PVA showed a major endothermic transition at 224.76°C. Both values are consistent with their respective reported melting ranges of 300–350°C, indicating no significant thermal degradation during the analysis. The thermogram of the physical mixture displayed peaks corresponding to Metronidazole, Eudragit RS-100, and PVA without any noticeable shift or disappearance of peaks. This observation suggests the absence of significant interactions between the drug and excipients, indicating compatibility and suitability for formulation development.

Formulation Design

Different formulation batches of nanosponges were systematically created using RSM based factorial design approach. The independent process variables in this design were the concentration of Eudragit RS-100 (X1), the quantity of PVA (X2), and the stirring speed (X3). Table 4 summarizes the various components and their respective levels. To assess the impact of these factors, particle size measured in nanometers (Y1), entrapment efficiency denoted as %EE (Y2), and percentage drug release (Y3) were designated as the dependent response parameters.

Data Analysis for Optimization and Model Validation

Data Model Fitting

The three independent variables, presented at lower, medium, and higher design points in both coded and uncoded forms, are shown in the following tables. All responses derived from the 20 unique formulations were analyzed and adapted to a quadratic effect model. This model was identified as the most suitable fit for Y1, Y2, and Y3, as assessed by Design Expert® software (Table 5). The ANOVA results shown in Table 7 demonstrate that the used model was statistically significant for all dependent variables.

The study demonstrated that the independent variables X1 (mg), X2 (mg), and X3 (RPM) had a beneficial effect on the synthesis of nanosponges.

Regression Equations

$Y1=349.64+17.12A+33.63B+28.37C-8.83AB-6.14AC-18.75BC-22.79A^2-4.96B^2-5.76C^2$ ---------- (1)

$Y2=81.90-0.25A-0.16B-0.09C+0.40AB+0.52AC+0.52BC+0.68A^2+0.44B^2+0.68C^2$----------(2)

$Y3=91.95-0.10A-0.12B-0.26C+0.39AB+0.56AC+0.21BC+0.51A^2+0.57B^2+0.39C^2$----------(3)

The polynomial regression equations Y_1, Y_2, and Y_3 describe the relationships between the dependent variables (Y_1, Y_2, and Y_3) and the independent variables (A, B and C), including their linear, interaction (ABC), and quadratic effects. These equations demonstrate how changes in A, B and C, individually and in combination, influence Y_1, Y_2, and Y_3, with quadratic terms accounting for non-linear variations.

Evaluation of Models for Dependent Variables

Upon inputting the experimental data into Design Expert® software, the Fit Summary suggested that a Quadratic Model was most suitable for all responses. Statistical analysis was performed using ANOVA, and the results for the evaluated responses are summarized below. For the first response, the overall model was significant with an F-value of 10.15 and a p-value of 0.0006. Individual factor analysis revealed that Eudragit RS-100 (A) had an F-value of 8.72 and p = 0.0145, PVA (B) had an F-value of 33.64 and p = 0.0002, and swirling speed (C) showed an F-value of 23.94 and p = 0.0006. Interaction terms AB and AC were non-significant ($p > 0.05$), while BC was significant (F = 6.13, p = 0.0328). Quadratic terms A^2 was significant (F = 16.30, p = 0.0024), while B^2 and C^2 were non-significant. The residual sum of squares was 4590.89, and lack of fit was non-significant with F = 78.32 and $p < 0.0001$.

For the second response, the model was also significant (F = 10.86, p = 0.0004). Eudragit RS-100 (A) showed a near-significant effect (F = 4.23, p = 0.0668), while PVA (B) and swirling speed (C) were non-significant. Interaction terms AB, AC, and BC were significant, with p-values of 0.0318, 0.0092, and 0.0092, respectively. Quadratic terms A^2, B^2, and C^2 were all highly significant ($p < 0.005$), indicating strong non-linear effects. Residual analysis showed a sum of squares of 2.10, and the lack of fit was not significant (F = 1.45, p = 0.3459).

In the third response, the overall model was significant with F = 9.05 and p = 0.0010. Among the individual factors, swirling speed (C) was significant (F = 5.16, p = 0.0465), while A and B were non-significant. Interaction terms AB and AC were significant (F = 6.99, p = 0.0246 and F = 14.26, p = 0.0036, respectively), while BC was not

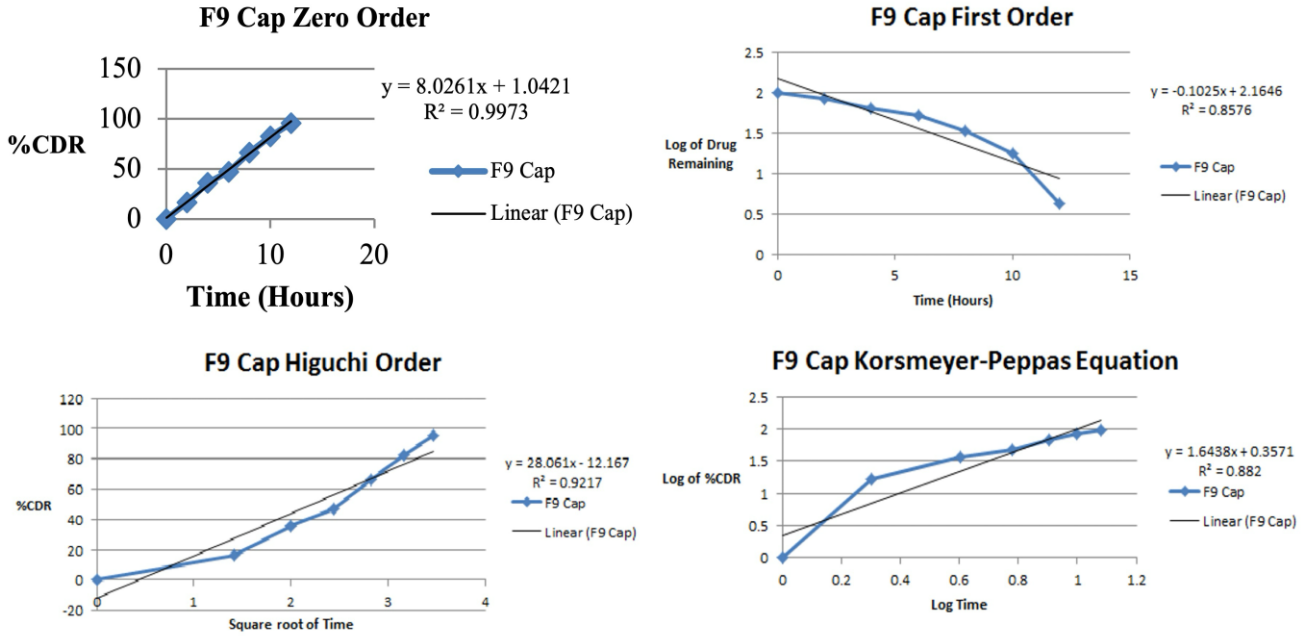

Figure 9: Kinetics of F9 Cap

Table 8: Pre-Compression Parameters of Nanosponges

Batch Code	BD (gm/ml)	TD (gm/ml)	Carr's Index (%)	Hausner Ratio	θ
F-1	0.50 ± 0.03	0.60 ± 0.03	16.67 ± 0.02	1.20 ± 0.03	25.10 ± 0.11
F-2	0.48 ± 0.03	0.58 ± 0.03	17.24 ± 0.02	1.21 ± 0.03	24.80 ± 0.23
F-3	0.52 ± 0.02	0.65 ± 0.03	20.00 ± 0.02	1.25 ± 0.03	24.95 ± 0.21
F-4	0.51 ± 0.03	0.64 ± 0.02	20.31 ± 0.03	1.26 ± 0.04	24.50 ± 0.21
F-5	0.49 ± 0.04	0.63 ± 0.02	19.05 ± 0.04	1.23 ± 0.03	26.10 ± 0.22
F-6	0.47 ± 0.04	0.62 ± 0.02	24.19 ± 0.03	1.32 ± 0.03	27.20 ± 0.21
F-7	0.46 ± 0.03	0.61 ± 0.03	22.95 ± 0.03	1.30 ± 0.04	25.75 ± 0.18
F-8	0.50 ± 0.03	0.57 ± 0.03	21.12 ± 0.02	1.22 ± 0.03	23.80 ± 0.11
F-9	0.57 ± 0.03	0.65 ± 0.03	12.31 ± 0.02	1.14 ± 0.03	22.80 ± 0.23
F-10	0.49 ± 0.02	0.61 ± 0.03	19.67 ± 0.02	1.24 ± 0.03	25.00 ± 0.21
F-11	0.48 ± 0.03	0.60 ± 0.02	20.00 ± 0.02	1.25 ± 0.03	25.80 ± 0.20
F-12	0.50 ± 0.04	0.59 ± 0.02	15.25 ± 0.04	1.18 ± 0.03	26.00 ± 0.22
F-13	0.46 ± 0.04	0.62 ± 0.02	22.00 ± 0.03	1.28 ± 0.03	22.50 ± 0.21
F-14	0.48 ± 0.03	0.63 ± 0.02	21.25 ± 0.02	1.27 ± 0.03	25.50 ± 0.20
F-15	0.49 ± 0.03	0.64 ± 0.02	21.88 ± 0.03	1.28 ± 0.03	25.90 ± 0.18
F-16	0.52 ± 0.02	0.66 ± 0.03	21.21 ± 0.02	1.27 ± 0.04	25.25 ± 0.19
F-17	0.47 ± 0.03	0.63 ± 0.03	19.42 ± 0.03	1.24 ± 0.03	23.95 ± 0.22
F-18	0.50 ± 0.03	0.64 ± 0.02	21.88 ± 0.03	1.28 ± 0.04	25.70 ± 0.21
F-19	0.48 ± 0.04	0.62 ± 0.02	22.58 ± 0.04	1.29 ± 0.03	26.10 ± 0.22
F-20	0.49 ± 0.04	0.61 ± 0.02	19.67 ± 0.03	1.24 ± 0.03	24.80 ± 0.21

Table 9: Formulation of Capsule using optimized nanosponges

Name of Ingredients	F9 Quantity
Nanosponges Formulation	
Nanosponges contain (Metronidazole:15mg; Eudragit RS-100: 100mg; and PVA: 50mg)	165mg
Capsule Formulation	
Nanosponges equivalent (Metronidazole 15mg) for 1 Capsule	165mg

Table 10: Evaluation of Capsule containing nanosponges

Batch Code	Uniformity of Content	% Drug content
F9 Cap	0.1905 ± 0.03	99.15 ± 0.02

Table 11: Drug release profile of F9 Capsule

Time (Hours)	F9 Cap
0	0
2	16.51 ± 0.05
4	36.06 ± 0.09
6	47.20 ± 0.03
8	66.40 ± 0.04
10	82.52 ± 0.06
12	95.70 ± 0.01

significant. Quadratic terms A^2, B^2, and C^2 were all significant, showing non-linear contributions to the response. The residual sum of squares was 1.75, and the lack of fit was non-significant ($F = 2.40$, $p = 0.1789$).

Overall, these ANOVA results demonstrate that the interactions between formulation factors and their quadratic effects play a crucial role in influencing the dependent variables. The findings highlight that factor effects are not purely linear and that altering multiple factors simultaneously at different levels can result in varying degrees of response, which justifies the use of a quadratic model for optimization.

Response Surface Plot (RSP) Analysis

3D RSPs were created using Design Expert® software, and the resulting graphical outputs are shown in Figure 4 for the assessed responses: Particle size (nm) (Y1), Entrapment Efficiency (%EE) (Y2), and %Drug Release (Y3). Furthermore, Figure 4 depicts the response surface depiction demonstrating the effect of Eudragit RS-100 concentration (X1), PVA (X2), and swirling speed (X3) on particle size (Y1). Among the several design batches, the nanosponge formulation exhibiting the most favorable and appropriate particle size was deemed preferable and hence chosen as the optimized formulation batch. The smallest particle size was observed in F09 (200.78 nm), which contained coded concentrations of X_1, X_2 and X_3. This indicates that a balanced concentration of X_1, X_2 and X_3 might result in more stable particle formation, minimizing aggregation and producing smaller particles. The results suggest that an optimal ratio of X_1, X_2 and $X_3$is crucial for controlling particle size.

Figure 4 shows RSP of Eudragit RS-100 concentration (X_1) and PVA (X_2) (%EE) (Y_2) and %CDR (Y_3). To determine the optimized batch, we need to balance high entrapment efficiency (%EE), desirable particle size (Y1), and high cumulative drug release (%CDR). Among all formulations, Formulation F9 (X1 = 100 mg, X2 = 50 mg, X3 = 500 RPM) delivers the best results for both Y2 (85.95%) and Y3 (95.15%). The analysis shows that X2 = 50 mg and higher RPM (1000) contribute to better Y3 values, while lower RPM (500) and X2 = 50 mg are linked with higher Y2 values. Increasing X1 or reducing X3 RPM does not consistently improve the responses. Therefore, a combination of lower X1 (100 mg), lower X2 (50 mg), and moderate RPM (500–1000) optimizes both Y2 and Y3.

The quadratic model exhibited statistically significant outcomes, with the p-value found to be below 0.05.

Furthermore, the analysis was validated through ANOVA testing, which also indicated a significant effect.

Evaluation of Optimized Nanosponges Formulation

Particle Size, ZP, and Polydispersity Index (PDI)

The improved formulation (F9) exhibited nanosized particles that remained uniformly distributed in the medium owing to robust repulsive interactions, as seen in Figure 5. The average particle size was determined to be 200.78 nm, the ZP was -31.7 mV, and the formulation had a narrow size distribution with a PDI of 0.205.

% EE and Drug Loading Capacity (%DL)

The drug %EE and %DL capacities of all the nanosponges (F1-F20) were determined between 81.55±1.28 to 85.95±0.95% and 70.25±0.10 to 79.53±0.13%, respectively, and are shown in Table 6.

XRD Analysis

The successful formation of METRO nanosponges was confirmed, as demonstrated in Figure 6, where the XRD pattern of the METRO nanosponges displayed a noticeably smoother curve when compared with that of the purified substance.

DSC Analysis

An endothermic melting transition was observed at 147.74 ºC in the DSC profile of the pure METRO compound. Conversely, the METRO nanosponges demonstrated integration into the amorphous nanosponge matrix, as seen in Figure 7. The thermal characteristics of the nanosponge exhibited an endothermic peak at 208.67 ºC, which is in closer proximity to the thermal peak associated with E-RS100.

SEM Analysis

Based on the observations from SEM analysis, the nanosponge formulation (F9) exhibited particle sizes within the range of 200–385 nm. As illustrated in Figure 8, the surface morphology of the nanosponges appeared smooth and free from any visible crystalline drug residues, while the particle diameters across all prepared formulations were found to remain stable and consistent.

In-vitro Drug Release Study

The dissolution behavior of METRO nanosponges (F9) was evaluated employing a USP-II type dissolution apparatus, maintained at a controlled temperature of 37±0.5ºC and operated at a paddle speed of 100 rpm in phosphate buffer medium with pH 6.8. Aliquots were systematically withdrawn at predetermined intervals of 0, 2, 4, 6, 8, 10, and 12 hours. The cumulative drug release for the tested formulations was observed to fall within the range of 92.74±1.09% to 95.15±1.20% over the 12-hour period, as summarized in Table 7.

Preformulation Studies of Nanosponges

The flow properties, such as angle of repose (θ), bulk density (BD), tapped density (TD), and compressibility index, were analyzed for the improved formulations to evaluate their suitability for nanosponge preparation. The F9 optimized batch showed improved flow behavior compared to the other formulations, which had somewhat moderate flow parameters, as illustrated in Table 8.

Formulation of Capsule using Optimized Nanosponges

The improved nanosponge formulation (F9) was encapsulated in hard gelatin capsules. Each capsule was engineered to hold a notional medication load of 15 mg of Metronidazole. For comparative analysis, an extra batch of capsules was made with just the pure medication, excluding any polymeric carrier. The dissolving profiles of both capsule types were then assessed, with the findings shown in Table 9 and Table 10.

Table 12: Stability analysis of variables of the improved formulation (F9)

Parameters	Initial Month	1st Month	2nd Month	3rd Month
Physical Appearance	No Change			
Drug Content	99.15 ± 0.02	99.10 ± 0.02	98.85 ± 0.02	98.50 ± 0.02
Dissolution (%)	95.70 ± 0.01	95.50 ± 0.01	94.80 ± 0.01	94.10 ± 0.01

Evaluation of Capsule

In-vitro Dissolution

The *in-vitro* dissolution test of the formulated capsules was conducted using a buffer solution at pH 6.8. The results demonstrated that formulation F9 had an optimum and sustained drug release profile over 12 hours, as shown in Table 11.

Drug Release Kinetics

Figure 9 illustrates the release kinetics study for the F9 formulation. The experimental data from the *in-vitro* release profile of the improved F9 batch were analyzed using several existing kinetic models to ascertain the mechanism driving drug release from Metronidazole-loaded nanosponges. A robust linear correlation was seen with the zero-order model ($R^2 = 0.9973$), indicating that the synthesized nanosponges facilitated a uniform and regulated drug release over a period of 12 hours. The Higuchi model ($R^2 = 0.9217$) exhibited significant linearity, indicating that the diffusion process was crucial in regulating the release rate. The release pattern of the improved formulation conformed most closely to the Higuchi model, concurrently demonstrating a zero-order drug release mechanism.

Accelerated Stability Study

The improved capsule formulations were assessed for stability, and the results are given in Table 12. The data suggest that the capsule from formulation batch F9 exhibited adequate stability when maintained under the designated temperature and humidity conditions, confirming its appropriateness as a stable formulation.

CONCLUSION

This work effectively illustrated the creation of Metronidazole-loaded nanosponges characterized by optimal nanoscale dimensions, increased entrapment efficiency, and a prolonged drug release profile. The improved formulation (F9) demonstrated uniform particle dispersion, stability, and constant drug release according to zero-order kinetics, signifying regulated release behavior. The capsule formulation of the nanosponges validated the potential for converting the formulation into a patient-friendly dose form with prolonged stability. Nanosponge-based systems provide a potential drug delivery platform to enhance the solubility, bioavailability, and therapeutic efficiency of poorly soluble medicines such as Metronidazole.

Acknowledgments

The authors express gratitude to the DIST-FIST Project (File No. DST FIST-2015; File No. SR/FST/College-272), Department of Science & Technology, New Delhi, Rajiv Gandhi Science & Technology Commission (RGSTC), Mumbai, and AICTE (MODROB) for their financial support in the central instrumentation facility at SRES, Sanjivani College of Pharmaceutical Education and Research (Autonomous), Kopargaon, India, for this research work.

REFERENCES

1. Hakim LK, Yazdanian M, Alam M, Abbasi K, Tebyaniyan H, Tahmasebi E, et al. Biocompatible and Biomaterials Application in Drug Delivery System in Oral Cavity. Evid Based Complement Alternat Med. 2021;2021:9011226.
2. Ouyang J, Zhang Z, Deng B, Liu J, Wang L, Liu H, et al. Oral Drug Delivery Platforms for Biomedical Applications. Mater Today. 2023;62:296–326.
3. He H, Lu Y, Qi J, Zhu Q, Chen Z, Wu W. Adapting Liposomes for Oral Drug Delivery. Acta Pharm Sin B. 2019;9(1):36–48.
4. Alqahtani MS, Kazi M, Alsenaidy MA, Ahmad MZ. Advances in Oral Drug Delivery. Front Pharmacol. 2021;12:618411.
5. Lou J, Duan H, Qin Q, Teng Z, Gan F, Zhou X, Zhou X. Advances in Oral Drug Delivery Systems: Challenges and Opportunities. Pharmaceutics. 2023;15(2):484.
6. Dingsdag SA, Hunter N. Metronidazole: An Update on Metabolism, Structure-Cytotoxicity and Resistance Mechanisms. J Antimicrob Chemother. 2018;73(2):265–279.
7. Ellis C, Odunayo A, Tolbert MK. The Use of Metronidazole in Acute Diarrhea in Dogs: A Narrative Review. Top Companion Anim Med. 2023;56–57:100824.
8. Afzal A. Bal AM. Metronidazole. Compr Pharmacol Seven Vol. set. 2022;7(V7):313-V7:321.
9. Wang YL, Gómez-Avilés A, Zhang S, Rodriguez JJ, Bedia J, Belver C. Metronidazole Photodegradation under Solar Light with UiO-66-NH2 Photocatalyst: Mechanisms, Pathway, and Toxicity Assessment. J Environ Chem Eng. 2023;11(3).
10. Sørensen CG, Karlsson WK, Amin FM, Lindelof M. Metronidazole-Induced Encephalopathy: A Systematic Review. J Neurol. 2020;267(1):1–13.
11. Hernández Ceruelos A, Romero-Quezada LC, Ruvalcaba Ledezma JC, López Contreras L. Therapeutic Uses of Metronidazole and Its Side Effects: An Update. Eur Rev Med Pharmacol Sci. 2019;23(1):397–401.
12. Iravani S, Varma RS. Nanosponges for Drug Delivery and Cancer Therapy: Recent Advances. Nanomaterials (Basel). 2022;12(14):2440.
13. Utzeri G, Matias PMC, Murtinho D, Valente AJM. Cyclodextrin-Based Nanosponges: Overview and Opportunities. Front Chem. 2022;10:859406.
14. Iravani S, Varma RS. Nanosponges for Water Treatment: Progress and Challenges. Appl Sci. 2022;12(9).
15. Zhang Q, Honko A, Zhou J, Gong H, Downs SN, Vasquez JH, et al. Cellular Nanosponges Inhibit SARS-CoV-2 Infectivity. Nano Lett. 2020;20(7):5570–5574.
16. Bhowmik H, Venkatesh DN, Kuila A, Kumar KH. Nanosponges: A Review. Int J Appl Pharm. 2018;10(4):1–5.
17. J A, Girigoswami A, Girigoswami K. Versatile Applications of Nanosponges in Biomedical Field: A Glimpse on SARS-CoV-2 Management. BioNanoScience. 2022;12(3):1018–1031.
18. Sherje AP, Dravyakar BR, Kadam D, Jadhav M. Cyclodextrin-Based Nanosponges: A Critical Review. Carbohydr Polym. 2017;173:37–49.
19. Utomo SB, Prabawati SY, Wahyuni I, VH ES, Mulyani S, Setyowati WA, et al. Inhibition Profile of Calix (4) Resorcinarene against Formation of Calcium Sulfate. Adv J Chem. 2025;8(12)(A):1876–1889.
20. Dullah AAM, Daud A, Mallongi A, Zakir M, Jafar N, Indar, et al. Microplastics in Marine Biota and Human Health Risk in the Coastal Area. Adv J Chem Sect A. 2025;8(8):1329–1343.
21. Abed AA, Banimuslem HA, Hassoni MH. Preparation of Copper Oxide Nanoparticles and Measurement of Their Effect on Bacterial Biofilm Formation. Adv J Chem Sect A. 2025;8(6):1043–1054.
22. Akib S, Faizan S, Ahmed A, Khan GJ. Development and Physicochemical Characterization of Solid Lipid Nanoparticles Containing Tinidazole. J PharmSci Comput Chem. 2023;1(3):88–95.
23. Soumya P, Sofi SI, Vignanandam S, Aishwarya B, Kholi CB, Anusha K, et al. A Study to Assess the Efficacy of Various Therapeutic Strategies Used in the Treatment of Psoriasis. J PharmSci Comput Chem. 2025;1(1):38–49.
24. Prohit PV, Pakhare PS, Pawar VB, Dandade SS, Waghmare MS, Shaikh FA, et al. Formulation and Comparative Evaluation of Naproxen-Based Transdermal Gels. J PharmSci Comput Chem. 2025;1(2):83–105.
25. Gopalaiah SB, Jayaseelan K. Quality-by-Design Guided Development, Optimization and Characterization of Irbesartan-Loaded Chitosan Nanoparticles: A Novel Antihypertensive Drug Delivery System. J Med Pharm Chem Res. 2025;7(11):2574–2595.
26. Reddy SH, Manimaran V. *In-Vitro* and *in-Vivo* Evaluation of Doxycycline Hyclate and Piroxicam Loaded Chitosan Nanoparticles into Transdermal Patch for Healing Diabetic Foot Ulcer. J Med Pharm Chem Res. 2025;7(3):357–383.
27. Susanti G, Aldi Y, Handayani D, Ismed F, Setiawansyah A. Chemical and Pharmacological Potential of Ficus elastica Fractions for Anti-hyperlipidemia: An Integrative Analysis from Molecular Docking, *In Vitro*, and *in Vivo* Studies. Chem Methodol. 2025;9(8):691–701.
28. Çakar E, Çakar S, Toibazarova A, Syzdykbayev M, Sydykova G, Appazov N, et al. Dye Sensitized Solar

Cells Applications of Ruhemann's Purple Metal Complexes. Chem Methodol. 2025;9:1143–1153.
29. Bajaj H, Sobuj DR, Qureshi MS, Sharma N, Singh LP, Boggula N, et al. Green Extraction and *in Vivo* Screening of Myrica Nagi Bark for Antidepressant, Antidiabetic, and Analgesic Potentials. Asian J Green Chem. 2026;10:69–83.
30. Shah PA, Syed HK, Sohail AR, Pervaiz A, Iqbal MS, Liew KB, et al. Comparison of Solvent Evaporation and Ultrasonic-Assisted Production Methods in the Development of Nimesulide Nanosponges and Their Characterization. Trop J Pharm Res. 2022;21(6):1139–1145.
31. Pawar Y A, R. Jadhav K, Rao JB, Tapkir AD, Malpure PS, Bachhav RS. Development and Characterization of Griseofulvin Nanosponges to Enhance Bioavailability. Int J Life Sci Pharma Res. 2022;P99–111.
32. Shaikh SS, Deshmukh SA, Satpute RB, Pawar VV, Gangurde HH. Formulation and Evaluation of Green Tea-Based Herbal Anti-aging Cream for Effective Skin Care. J PharmSci Comput Chem. 2025;1(2):69–82.